Heliyon 8 (2022) e09665

Contents lists available at ScienceDirect

Heliyon

journal homepage: www.cell.com/heliyon

Research article

Metabolome and transcriptome analysis of eleutheroside B biosynthesis pathway in *Eleutherococcus senticosus*

Hong-Yu Guo [a], Jie Zhang [a], Li-Mei Lin [a], Xin Song [a], Duo-Duo Zhang [a], Ming-Hui Cui [a], Chang-Wen Long [b], Yue-Hong Long [a,**], Zhao-Bin Xing [a,*]

[a] College of Life Sciences, North China University of Science and Technology, Tangshan, China
[b] Hebeidingzhou High School, Dingzhou, China

ARTICLE INFO

Keywords:
Eleutheroside B
Eleutherococcus senticosus (Ruper. et Maxim.) Maxim
Young stage
Metabolome
Transcriptome

ABSTRACT

Eleutheroside B (syringin) is a medicinal active ingredient extracted from *Eleutherococcus senticosus* (Ruper. et Maxim.) Maxim with high clinical application value. However, its synthesis pathway remains unknown. Here, we analyzed the eleutheroside B biosynthesis pathway in *E. senticosus*. Consequently, metabolomic and transcriptomic analyses identified 461 differentially expressed genes (DEGs) and 425 metabolites. Further, we identified 7 DEGs and 67 metabolites involved in the eleutheroside B biosynthetic pathway in the eleutheroside B high and low plants. The correlation between the gene and metabolites was explored using the pearson correlation coefficient (PCC) analysis. Caffeoyl-CoA O-methyltransferase, caffeic acid-O-methyltransferase, β-amyrin synthase (β-AS) genes, NAC5, and HB5 transcription factors were identified as candidate genes and transcription factors related to the eleutheroside B synthesis. Eleutheroside B content was the highest at the young stage of the leaves both in the high and low eleutheroside B plants. Quantitative real-time polymerase chain reaction revealed that phenylalanine ammonia-lyase1, cinnamate 4-hydroxylase, *β-AS*, and leucoanthocyanidin reductase gene had higher expression levels at the young stage of the leaves in the low eleutheroside B plants but lower expression levels in the high eleutheroside B plants. In the present study, we complemented the eleutheroside B biosynthetic pathway by analyzing the expression levels of relevant genes and metabolite accumulation patterns.

1. Introduction

Eleutherococcus senticosus (Ruper. et Maxim.) Maxim. also as "ciwujia" in China or "Siberian ginseng" in Western countries is a woody plant belonging to the *Araliaceae* species and an essential medicinal plant in China. Its stems and leaves have medicinal value, including anti-inflammatory and hypoglycemic effects (The State Pharmacopoeia Commission of P.R. China, 2015). *E. senticosus* leaves are used to produce *E. senticosus* tea (ci-wu-jia tea) (Huang et al., 2017) or added into dishes. Therefore, *E. senticosus* is a healthy food with medicine and food homology (Zhang, 2009). *E. senticosus* primarily thrives in Liaoning, Jilin, Heilongjiang, Hebei Provinces (China) and Russia, South Korea, and Japan (Huang et al., 2011). It has several active chemical constituents, including lignans, triterpenoid saponins, flavonoids, polysaccharides. Triterpenoids, flavonoids, and lignans are the primary secondary metabolites of *E. senticosus* (Wang et al., 2013). The candidate genes participating in the triterpenoid biosynthetic pathway of *E. senticosus* have been revealed with transcriptome sequencing (Song et al., 2016; Hwang et al., 2015). Lignans and flavonoids in *E. senticosus* have also been explored (Wu et al., 2018). The difference in the content of protocatechuic acid, eleutheroside B, eleutheroside E, isofraxidin, hyperoside, kaempferol, and oleanolic acid between *E. senticosus* and *E. sessiliflorus* has been explored via comparative metabolomics (Wu et al., 2018). Emerging studies on the triterpenoid saponins biosynthetic pathway include key gene cloning, saponins content trend at different developmental stages, and the effect of DNA methylation on triterpenoid saponins (Guo et al., 2017; Xing et al., 2012; Long et al., 2015; Wang et al., 2019). Nevertheless, only content measurement and extraction in different organs or periods have been reported in eleutheroside B (Li and Fu et al., 2019; Meng et al., 2009).

Eleutheroside B is produced via the phenylpropanoid biosynthetic pathway, starting from L-phenylalanine. Nonetheless, the eleutheroside B biosynthetic pathway is unknown. Thus, it is imperative to explore key enzymes and metabolites related to eleutheroside B biosynthesis. The

* Corresponding author.
** Corresponding author.
E-mail addresses: longyh@ncst.edu.cn (Y.-H. Long), xingzb@ncst.edu.cn (Z.-B. Xing).

https://doi.org/10.1016/j.heliyon.2022.e09665
Received 7 December 2021; Received in revised form 15 February 2022; Accepted 31 May 2022

currently proposed biosynthetic pathway begins with (Murthy et al., 2014) phenylalanine ammonia-lyase (PAL) mediated synthesis of cinnamic acid from L-phenylalanine. The cinnamic acid is then converted to eleutheroside B via cinnamate 4-hydroxylase (C4H), coumarate 3-hydroxylase (C3H), caffeic acid O-methyltransferase (COMT), ferulate 5-hydroxylase (F5H), caffeoyl-CoA O-methyltransferase (CCoAOMT), 4-coumarate: CoA ligase (4CL), cinnamoyl-CoA reductase (CCR), cinnamyl alcohol dehydrogenase (CAD) and glycosyltransferase (GT). Eleutheroside B is a monolignol glycoside used to establish the quality of traditional chinese medicinal materials in the Chinese Pharmacopoeia 2015 edition. It has several pharmacological effects, including anti-inflammatory (Zhang et al., 2020; Dai et al., 2021), hypoglycemic (Kim et al., 2017; Shen et al., 2020), hypnotic (Cui et al., 2015), anti-cancer (Lee et al., 2019), and anti-oxidant (Wang et al., 2020).

This study used transcriptomics and metabonomics profiles to identify differentially expressed genes (DEGs) participating in eleutheroside B biosynthetic pathway to explore the molecular mechanism of producing the content difference. Further, we analyzed the secondary metabolites to explore the content change trend between the samples. Gene expression was integrated with the metabolite accumulation to analyze candidate genes and transcription factors underlying the eleutheroside B synthesis. In addition, a multi-omics approach was applied to explore the eleutheroside B biosynthetic pathway, geared towards improving the quality of *E. senticosus*.

2. Materials and methods

2.1. Plant materials

Different developmental stages (young, mature, and ageing) leaf samples of 100 *E. senticosus* plants were collected from the Wulingshan Nature Reserve (40.29°N, 117.17°E) in Hebei Province of China in June 2019. *E. senticosus* leaf samples at the three developmental stages were obtained between mid-to-late July. Professor Zhao-Bin Xing identified and confirmed the leaves. Three biological replicate samples were collected from the leaves in all stages, frozen immediately in liquid nitrogen, and stored at -80 °C.

2.2. Eleutheroside B extraction and UPLC detection

E. senticosus leaf samples were dried at 60 °C then ground to powder. Leaf powder about 0.40 g (Supplementary Table 1), and 10 ml mixture of ethanol/water (7:1) were mixed and ultrasonically crushed using a digital ultrasonic cell disruptor (Branson Sonifier-250, Danbury, CT, USA) at 120W for 15 min. The crude extract was extracted using petroleum ether and water saturation n-butanol to eliminate pigment and impurities in the leaves. Subsequently, the extract was dried under vacuum, fully dissolved in methanol, and filtered through a 0.22 μm (JET BIOFIL, Guangzhou, China) filter membrane for ultra-high performance liquid chromatography (UPLC) analysis.

Eleutheroside B (3.20 mg), a standard compound was dissolved in 100 ml methanol to make a standard solution, used to generate a calibration curve ($Y = 1.76 \times 10^4X+69.3$, $R^2 = 0.999858$) (Supplementary Table 1). All samples were analyzed using the UPLC system (Waters, Massachusetts, MD, USA) with an ACQUITY UPLC BEN C_{18} column (1.7 μm, 2.1 mm × 50 mm, Waters). The temperature was maintained at 35 °C. The gradient elution solvents comprised mobile phase A (pure water) and mobile phase B (methanol). The gradient program included: 0 min, 95% A; 7 min, 65% A; 8 min, 65% A; 10 min, 95%A; 13 min, 95% A. The flow rate, the injection volume, and the detection wavelength were 0.25 ml/min, 1 μl, and 213 nm, respectively.

2.3. Widely targeted metabolome analysis

Widely targeted metabolome analysis was performed by Metware Biotechnology Co., Ltd. (Wuhan, China). The freeze-dried leaves were crushed using a mixer mill (MM 400, Retsch, Dusseldorf, Germany) with a zirconia bead at 30 Hz for 1.5 min. Leaf powder (0.1 g) was fully dissolved in 0.6 ml 70% aqueous methanol and overnight extracted at 4 °C. After centrifugation (10, 000×*g*) for 10 min, the extracts were filtered through a 0.22 μm filter membrane (SCAA-104, ANPEL, Shanghai, China) for UPLC- tandem mass spectrometry (MS/MS) analysis.

The UPLC-ESI-MS/MS system (UPLC, Shim-pack UFLC SHIMADZU CBM30A system; MS, applied Biosystems 4500 Q TRAP) was used to extract the samples. The gradient elution solvents comprised mobile phase A (pure water with 0.04% acetic acid) and mobile phase B (acetonitrile with 0.04% acetic acid). The gradient program conditions included: 0 min, 95% A; 10 min, 5% A; 11 min, 5% A; 12 min, 95% A; 12.1 min, 95% A; 15 min, 95% A. All samples were analyzed using the ACQUITY UPLC HSS T3 C18 column (1.8 μm, 2.1 mm × 100 mm, Waters). The temperature was maintained at 40 °C. The flow rate and the injection volume were 0.35 ml/min and 4 μl, respectively.

API 4500 Q TRAP mass spectrometry system was equipped with electrospray ionization (ESI) Turbo Ion-Spray interface operating in positive and negative ion mode and controlled with Analyst 1.6.3 software. The ESI source operation parameters included: An ion source, turbo spray (temperature of 550 °C); ion spray voltage (IS) at 5,500 V; ion source gas I (GSI) at 50 psi; gas II (GSII) at 60 psi; curtain gas (CUR) at 30 psi. The collision gas (CAD) was set at high and QQQ scans were acquired via multiple reaction monitoring (MRM) experiments with collision gas (nitrogen) at 5 psi. Declustering potential (DP) and collision energy (CE) for individual MRM transitions were further optimized. We monitored a specific set of MRM transitions based on the metabolites eluted within each period.

Qualitative analysis of metabolites was performed using secondary mass spectrometry data based on the self-built metware database (MWDB), MassBank (http://www.massbank.jp/), and Metlin (https://metlin.scripps.edu/). The earlier described MRM was applied to quantify the metabolites (Chen et al., 2013). The analyst 1.6.3 software was adopted to analyze the integration and calibration of the chromatographic peak. The data of chromatographic peak area was exported for storage.

Principal component analysis (PCA) and orthogonal partial least squares discriminant analysis (OPLS-DA) was used for metabolites. The variable importance in a project (VIP) of the OPLS-DA model was obtained. The differentially accumulated metabolites (DAMs) were selected when VIP≥1 and fold change ≥2 or fold change ≤0.5.

2.4. Total RNA extraction and transcriptome sequencing

The total RNA was extracted and purified using the RNAprep Pure Plant Kit (TIANGEN, Beijing, China). Nanodrop One (Thermo Fisher Scientific, Waltham, MA, USA) spectrophotometer and Agilent 2100 Bioanalyzer (Agilent Technologies, Santa Clara, CA, USA) were used to determine the purity, concentration, and quality of total RNA. cDNA library was constructed using RNA (3 μg) from each sample, then sequenced on Illumina NovaSeq 6000 platform. Adaptor sequences and low-quality reads were removed from raw reads. Clean data was obtained after filtering. The Q20, Q30, and GC content in the clean data were calculated. Trinity software (v2.8.5) was adopted to assemble sequences using clean data. Low expression transcripts were filtered to construct unigenes.

The unigenes were compared and annotated with NR, Swiss-Prot, Gene Ontology (GO), Eukaryotic Ortholog Groups (KOG), Kyoto Encyclopedia of Genes and Genomes (KEGG) databases using the BLAST software (v2.2.31+) with default parameters. TransDecoder software (v3.0.0) was applied to predict the coding sequence and amino acid sequence of the unigenes. The iTAK software was used to predict the transcription factors (TFs). The gene expression levels in each sample and fragments per kilobase of transcript per million mapped reads (FPKM) were estimated with RSEM. Differential expression analysis of the two plants was performed using the DESeq2 (v1.10.1) software R package.

Fold Change ≥2, false discovery rate (FDR) < 0.01 were defined as DEGs. GOSeq (v2.12) and KOBAS (v2.0) software were used for GO and KEGG pathway functional enrichment analyses of the DEGs. The genes, transcription factors, and transporters were identified through annotation information of NR, Swiss-Prot, and GO.

2.5. Quantitative real-time polymerase chain reaction

After extracting and purifying the total RNA, FastQuant RT Kit (with gDNase) (TIANGEN, Beijing, China) was used to synthesize cDNA. A total of nine genes were randomly selected to design specific primers using Primer 5.0 software (Supplementary Table 2). qRT-PCR was performed on Applied Biosystems 7900HT (Thermo Fisher Scientific, Waltham, MA, USA) using Talent qPCR PreMix (SYBR Green) (TIANGEN, Beijing, China). The amplification reaction conditions were as follows: 95 °C for 3 min, followed by 40 cycles at 95 °C for 5 s, 60 °C for 10 s. Each sample was processed in three independent biological replicates with the *GAPDH* gene as the reference. The relative expression level of the gene was calculated using the $2^{-\Delta\Delta Ct}$ method (Livak and Schmittgen, 2001).

2.6. Statistical analysis

One-way ANOVA (Duncan's test) was used to establish the differences between the three developmental stage samples. $P < 0.05$ indicated a significant difference. Pearson correlation coefficient (PCC) was applied to establish the correlation between a pair of metabolites, genes, and metabolites. PCC>0.8, $P < 0.05$, and PCC>0.8, $P < 0.01$ were considered statistically significant between the correlation of pair of metabolites, metabolites, and genes, respectively. All analyses were performed using the SPSS 20.0 software. Cytoscape software (v3.7.2) was used for visualization.

3. Results

3.1. Analysis of metabolome differences between the eleutheroside B high and low eleutheroside B plants

We performed ultra-high performance liquid chromatography (UPLC) analysis of eleutheroside B on the samples which were mature stage leaves from 100 *E. senticosus* plants. The mature stage leaf samples which average eleutheroside B content (three replicate UPLC determinations) was 9.46 μg/g for 1–4 and 20.44 μg/g for 9–4, were screened (Supplementary Table 1). Then defined the plant which mature leaf eleutheroside B content 9.46 μg/g as the low eleutheroside B plants (plant 1) and the plant eleutheroside B content 20.44 μg/g as the high Eleutheroside B plant (plant 9), and subsequently analyzed eleutheroside B content of young leaves (9–2, 1–2) and ageing leaves (9–5, 1–5) of plants 9 and 1 (Supplementary Table 1), respectively, by ultra-high performance liquid chromatography. Metabolomics and transcriptome tests were performed on mature samples of high and low content plants; each sample was tested in three independent biological replicates.

Metabolome analysis was performed using the UPLC-ESI-MS/MS system to compare different metabolite accumulation between the high and low eleutheroside B plants. A total of 425 metabolites were identified in the high and low eleutheroside B plants (Supplementary Table 3). PCA revealed that the high and low eleutheroside B plants were significantly separated, indicating a difference between the two plants of metabolites (Supplementary Figure 1). OPLS-DA showed a significant difference in metabolites between the two plants (Supplementary Figure 2).

Based on KEGG and Plant Metabolic Pathway Databases (https://plantcyc.org/), metabolites are divided into six classifications, including secondary metabolites metabolism (151); amino acids metabolism (82); nucleotide metabolism (41); lipid metabolism (77); carbohydrate metabolism (28); and unclassified metabolites (55) (Supplementary Figure 3A; Supplementary Table 3) based on a metabolic pathway. Secondary metabolites metabolism can be further divided into phenylpropanoid metabolism (67) (ko00940), flavonoid metabolism (42) (ko00941, ko00943, ko00944), triterpenoid metabolism (14) (ko00909), benzoate degradation metabolism (8) (ko00362), benzoxazinoid biosynthesis (1) (ko00402), unclassified secondary metabolites metabolism (19) (ko00999) (Supplementary Figure 3B; Supplementary Table 3). Metabolites can be classified into diverse metabolism. For instance, cinnamic acid, p-coumaric acid, and chlorogenic acid participate in phenylpropanoid and flavonoid metabolisms.

A total of 26 DAMs were identified in the phenylpropanoid metabolism (Figure 1; Supplementary Table 4). Eleutheroside B is a final product synthesized in the phenylpropanoid metabolic pathway. Eleutheroside B increased 3.2-fold in the high eleutheroside B plants compared to the low eleutheroside B plants, this was consistent with previous content test results. The accumulation of six metabolites including eleutheroside E, fraxetin, and esculin was significantly higher in the high eleutheroside B plants than that in the low eleutheroside B plants. Skimmin content had the largest difference between the two plants; its accumulation was 4.2-fold higher in the high eleutheroside B plants than that in the low eleutheroside B plants. The accumulation of 19 metabolites including eleutheroside B1, isofraxidin, cryptochlorogenic acid, and syringaresinol was significantly higher in the low eleutheroside B plants than that in the high eleutheroside B plants. The content of 41 metabolites, including chlorogenic acid, sinapyl alcohol, caffeic acid, cinnamic acid, p-coumaric acid showed no significant difference in high and low eleutheroside B plants. All these metabolites were intermediate products of the phenylpropanoid metabolic pathway.

In total, 12 DAMs were identified in triterpenoid metabolism (Figure 2; Supplementary Table 4). Ciwujianoside C3 content was 1859.6-fold significantly higher in the high eleutheroside B plants than that in the low eleutheroside B plants. A total of nine DAMs, including ciwujianoside D1 and ciwujianoside B, had higher content accumulation in the high eleutheroside B plants than that in the low eleutheroside B plants. Accumulation of three metabolites including 2-hydroxyoleanolic acid was significantly higher in the low eleutheroside B plants than that in the high eleutheroside B plants. Ciwujianoside E and oleanolic acid-3-O-β-D-pyran xylose (1→3) -β-D-pyran glucuronide showed no significant difference in the high and low eleutheroside B plants.

A total of 23 DAMs were identified in the flavonoid metabolism (Figure 3; Supplementary Table 4). The content of catechin, prunetin, L-epicatechin, and apigenin-7,4′-dimethylether was more than 4-fold higher in the high eleutheroside B plants than that in the low eleutheroside B plants. L-epicatechin content had the largest difference with 7.9-fold. Rutin, cynaroside, hispidulin, and 13 metabolites showed significantly higher content in the low eleutheroside B plants than that in the high eleutheroside B plants. The content of 19 metabolites, including isotrifoliin, hyperin, and (-)-catechin gallate showed no significant difference in high and low eleutheroside B plants.

3.2. Analysis of DEGs involved in eleutheroside B biosynthetic pathway

The eleutheroside B biosynthetic pathway in plants is part of the phenylpropanoid metabolic pathway. The phenylpropanoid metabolic pathway includes the initial steps of the flavonoid metabolic pathway, lignin biosynthetic processes. *PAL*, *C4H*, 4CL, *HCT*, *COMT*, *CCR*, *CAD*, and other genes have been identified in the phenylpropanoid metabolic pathway (Supplementary Table 6). In the metabolome, we identified metabolites including chlorogenic acid, caffeic acid, cinnamic acid, p-coumaric acid, sinapoyl aldehyde, and sinapyl alcohol. The lignin and eleutheroside B biosynthetic processes. Meanwhile, by combining the lignin and current proposed eleutheroside B biosynthetic processes (Murthy et al., 2014; Dixon and Barros, 2019; Vanholme et al., 2019), we proposed an eleutheroside B biosynthetic pathway in *E. senticosus* (Figure 4). *PAL*-mediated synthesis of cinnamic acid from L-phenylalanine is the initial step, followed by *C4H*-mediated synthesis of p-coumaric acid from cinnamic acid. Synthesis of the p-coumaric acid pathway is divided into two major branches, i.e., the eleutheroside B biosynthetic

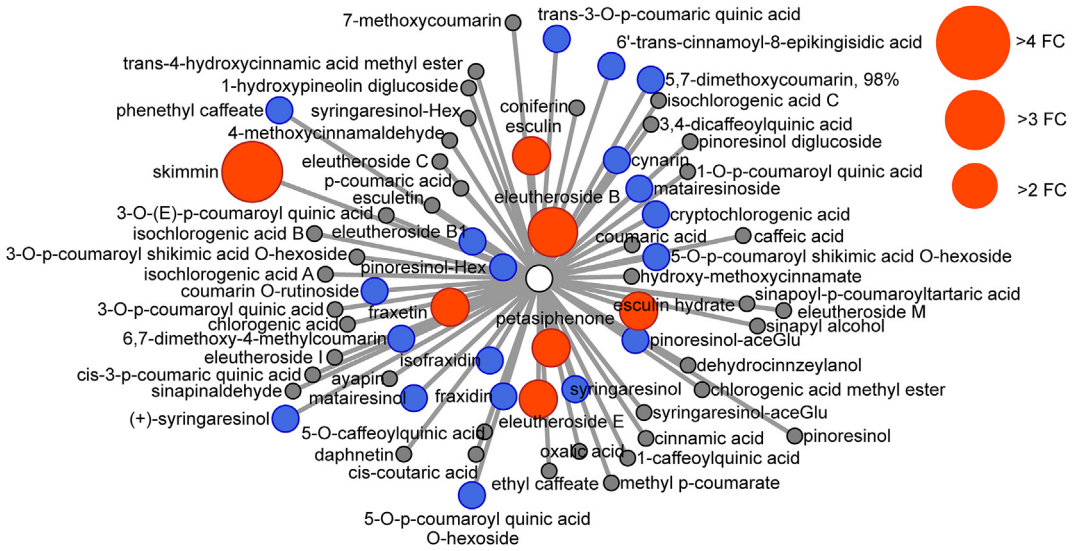

Figure 1. Metabolites involved in phenylpropanoid metabolism. Red and blue circles indicate significantly higher and lower (VIP>1) metabolite accumulation (VIP>1), respectively, in the high eleutheroside B plants than that in the low eleutheroside B plants. The Gray circle indicates no significant difference in the high and low eleutheroside B plants. Sizes of red circles represent fold change (FC).

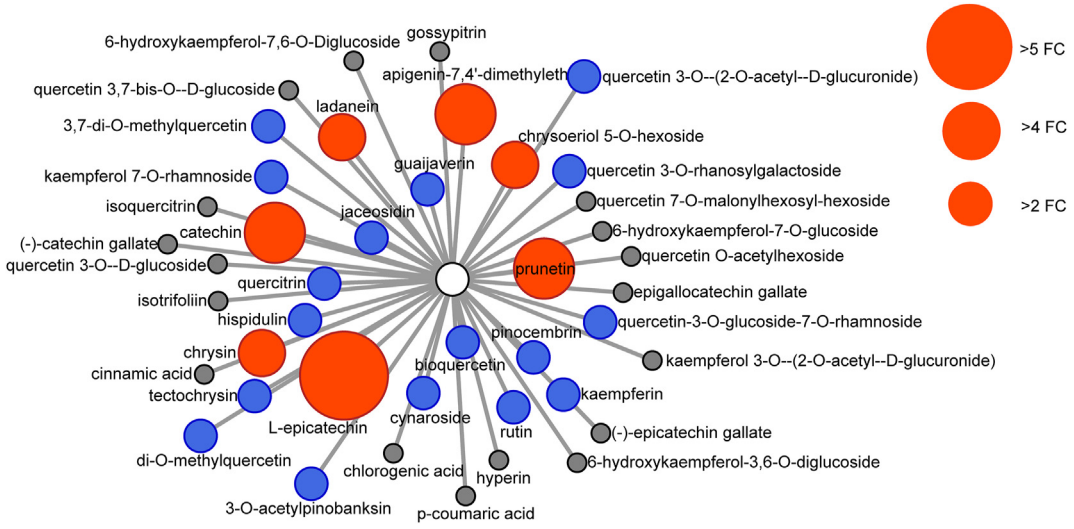

Figure 2. Metabolites involved in triterpenoid metabolism. Red and blue circles indicate significantly higher and lower (VIP>1) metabolite accumulation, respectively, in the high eleutheroside B plants than that in the low eleutheroside B plants. The Gray circle indicates no significant difference in the high and low eleutheroside B plants. Sizes of red circles represent fold change (FC).

pathway proposed by Murthy, involving nine types of enzymes implicated in the synthesis of eleutheroside B; and the second pathway inferred from references and catalyzed by various enzymes through different branch pathways. Seven DEGs including five genes annotated as *PAL* gene (*PAL1*, *PAL2*, *PAL3*, *PAL4*, and *PAL5*), one *C4H* gene, two *C3′H* genes (*C3′H1*, *C3′H2*), one *CSE* gene, one *CCoAOMT* gene, one *COMT* gene, one *CCR* gene were identified in eleutheroside B biosynthetic pathway (Supplementary Table 5). The seven DEGs showed higher expression levels in the high eleutheroside B plants than that in the low eleutheroside B plants. The gene expression levels and eleutheroside B content accumulation were higher in the high eleutheroside B plants than that in the low eleutheroside B plants.

A total of 461 DEGs were identified in the high and low eleutheroside B plants (Supplementary Table 6). Moreover, 377 DEGs were annotated. The DEGs were significantly enriched in 20 KEGG pathways, including phenylpropanoid, flavonoid, sesquiterpenoid, and triterpenoid biosynthetic pathways (Figure 5A). Meanwhile, DEGs were primarily enriched in three GO terms of molecular function, cellular component, and biological process (Figure 5B). The biological process included 11 terms, including cinnamic acid and lignin biosynthetic processes. The cinnamic acid and lignin biosynthetic processes belong to the phenylpropanoid metabolism and overlap on the eleutheroside B biosynthetic pathway. *PAL1*, *PAL3*, *PAL4*, and *PAL5* participate in the cinnamic acid biosynthetic process, whereas *C3′H2*, *CCoAOMT*, and *COMT* participate in the lignin biosynthetic process.

C4H, *C3′H1*, *C3′H2*, and *CCoAOMT* identified in the eleutheroside B biosynthetic pathway also participate in the flavonoid biosynthesis pathway. Leucoanthocyanidin reductase (*LAR*) gene was identified in flavonoid metabolism with different expression levels in the high and low eleutheroside B plants. The expression levels of the above five DEGs were upregulated more than 2-fold in the high eleutheroside B plants compared to that in the low eleutheroside B plants (Supplementary Figure 4; Supplementary Table 5). β-amyrin synthase (*β-AS*) and geranyl pyrophosphate synthase (*GPS*) genes were identified in triterpenoid

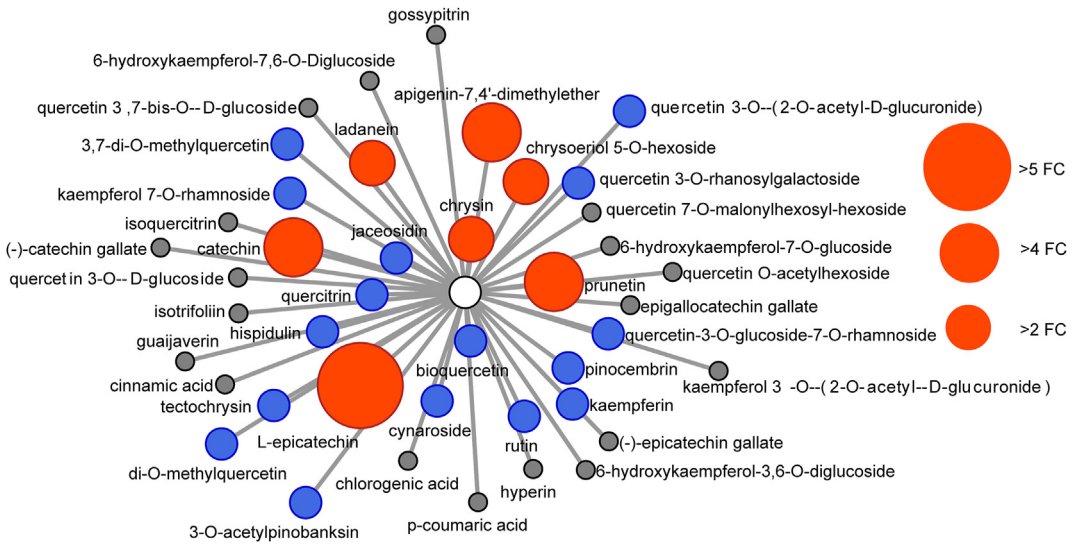

Figure 3. Metabolites involved in flavonoid metabolism. Red and blue circles indicate significantly higher and lower (VIP>1) metabolite accumulation, respectively, in the high eleutheroside B plants than that in the low eleutheroside B plants. The Gray circle indicates no significant difference in the high and low eleutheroside B plants. Sizes of red circles represent fold change (FC).

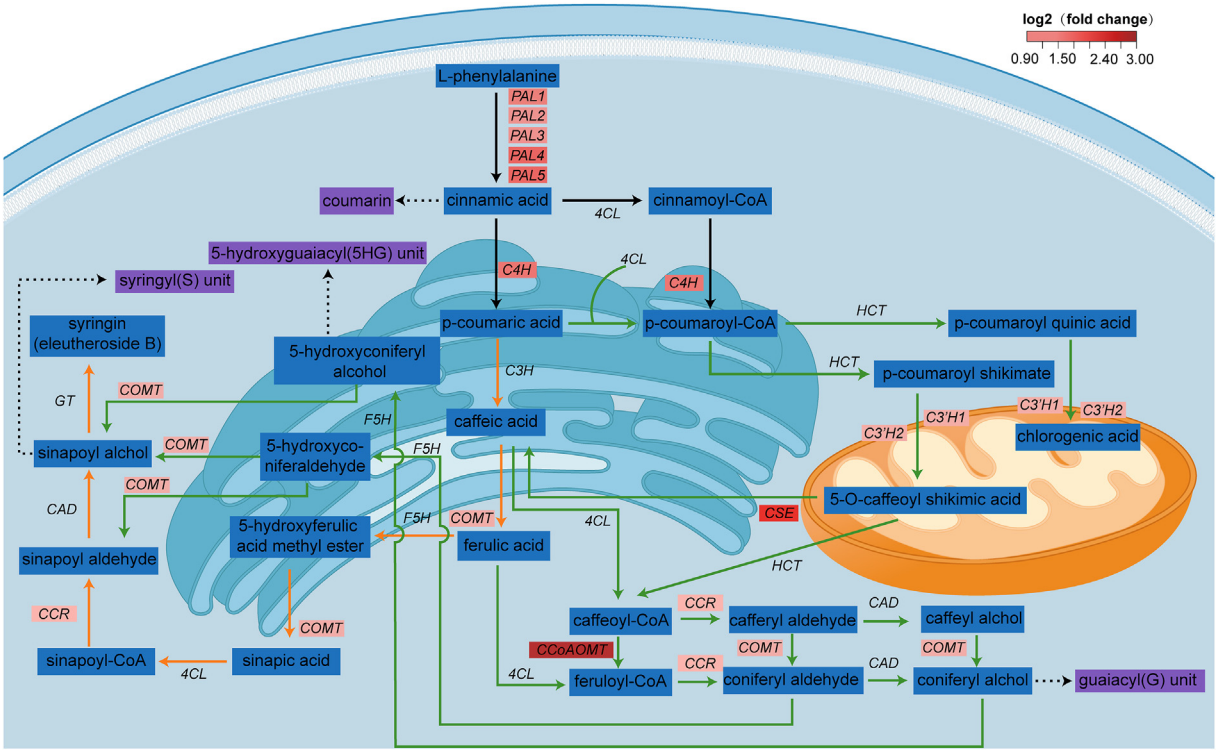

Figure 4. Eleutheroside B biosynthetic pathway. The route starting from L-phenylalanine along the orange line is the predicted pathway in other studies. The route starting from L-phenylalanine along the green line is the proposed pathway in this study. The red background cell above the line represents DEGs.

metabolism indicating different expression levels in the high and low eleutheroside B plants. *GPS* gene showed higher expression levels in the high eleutheroside B plants than that in the low eleutheroside B plants. In contrast, the *β-AS* gene expression level had a higher expression level in the low eleutheroside B plants (Supplementary Figure 4; Supplementary Table 5). A total of 19 DEGs encoding ABC transporters were identified in the eleutheroside B high and low eleutheroside B plants. The expression pattern is shown in Supplementary Figure 5 (Supplementary Table 7). A total of nine DEGs were randomly selected for qRT-PCR analysis. The expression pattern of DEGs was similar to that of transcriptome data (Supplementary Figure 6), implying the reliability of transcriptome data.

3.3. Correlation analysis between metabolites

PCC in the high and low eleutheroside B plants was used to analyze whether the change of metabolites accumulation was synergistic. A total of 67 metabolites participated in the phenylpropanoid metabolic pathway. Consequently, a significant correlation was observed between 64 metabolites in the high eleutheroside B plants (PCC>0.8, $P < 0.05$) (Figure 6A; Supplementary Table 8). However, out of the 67 metabolites, three metabolites, including eleutheroside B1, eleutheroside E, and 1-hydroxypineolin diglucoside were not correlated with other metabolites. On the other hand, a significant correlation was noted between the

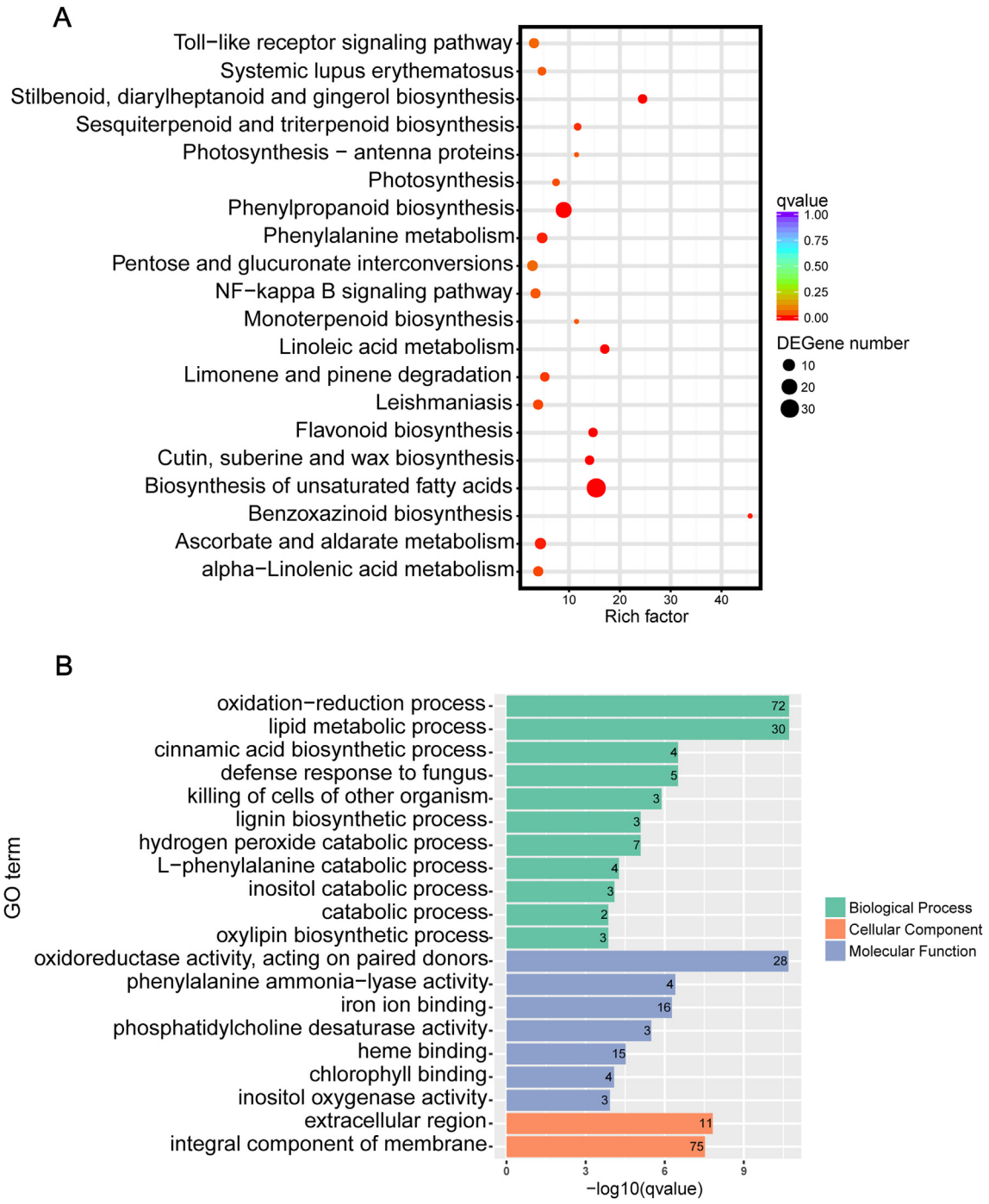

Figure 5. (A) DEGs enriched in 20 KEGG pathways; (B) DEGs enriched in 20 GO terms.

64 metabolites in the low eleutheroside B plants (PCC>0.8, $P < 0.05$) (Figure 6B; Supplementary Table 8). Whereas, three metabolites, including Cynarin, coniferin, and matairesinoside were not correlated with other metabolites. The correlation between the metabolites involved in phenylpropanoid metabolism was not consistent in the high and low eleutheroside B plants. Coumarin O-rutinoside showed a negative correlation with petasiphenone, pinoresinol-aceGlu, and other three metabolites in the high eleutheroside B plants, and was only correlated with sinapyl alcohol and 7-methoxycoumarin in the low eleutheroside B plants (Figure 7B). The correlating edges in the coumarin O-rutinoside and all metabolites (PCC>0.8) decreased in the low eleutheroside B plants. The correlation between the metabolites was also different. The 5-O-caffeoylquinic acid revealed a positive correlation with cis-3-p-coumaric quinic acid in the high eleutheroside B plants, while was negatively correlated in the low eleutheroside B plants.

A total of 42 metabolites participated in the flavonoid metabolic pathway. A significant correlation was noted between 40 metabolites in the high eleutheroside B plants (PCC>0.8, $P < 0.05$) (Figure 6C; Supplementary Table 9). Among the 42 metabolites, gossypitrin and quercetin 3-O-β-D-glucoside were not correlated with other metabolites. On the other hand, a significant correlation was detected between 36 metabolites in the low eleutheroside B plants (PCC>0.8, $P < 0.05$) (Figure 6D; Supplementary Table 9). Out of the 42 metabolites, L-epicatechin, tectochrysin, 3,7-di-O-methylquercetin, ladanein, quercetin O-acetylhexoside, and kaempferol 3-O-β-(2″-O-acetyl-β-D-glucuronide) were not correlated with other metabolites. A positive correlation was noted

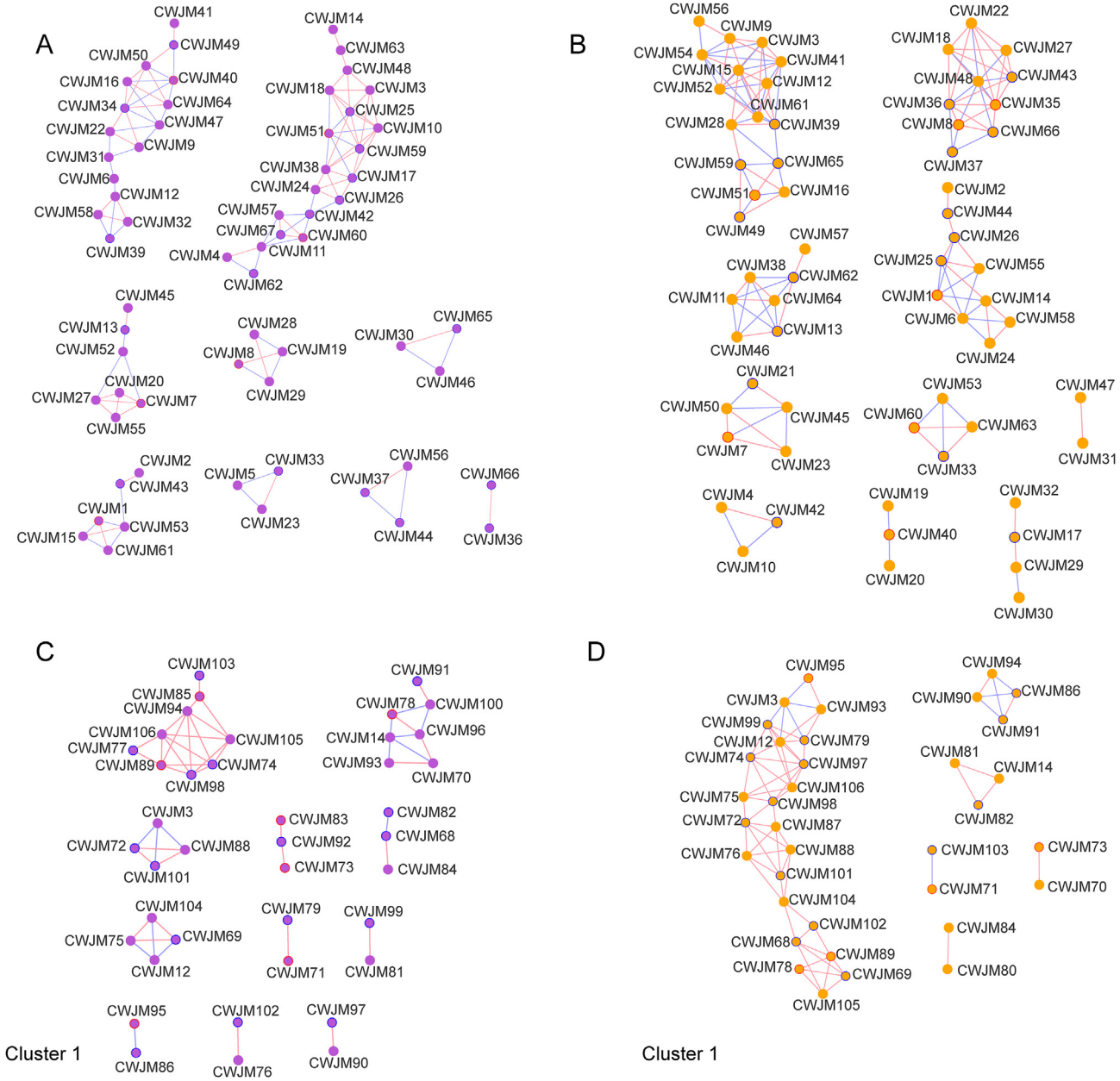

Figure 6. Correlation network between metabolites. Metabolites involved in phenylpropanoid metabolic pathway in the high (A), and low eleutheroside B plants (B). Metabolites involved in flavonoid metabolism pathway in the high (C), and low eleutheroside B plants (D). The circle with red and blue borders indicates significantly higher and lower (VIP>1) metabolite accumulation, respectively, in the high eleutheroside B plants than that in the low eleutheroside B plants. The circle without borders indicates no significant difference in the high and low eleutheroside B plants. Red and blue lines indicate significantly positive and negative correlations between metabolites, respectively.

between all metabolites in the high eleutheroside B plants in cluster 1 (Figure 6C). Chlorogenic acid showed a negative correlation with all metabolites in the low eleutheroside B plants, (PCC>0.8) in cluster 1, and was positively correlated with other flavonoid metabolites (Figure 6D). Notably, P-coumaric acid, cinnamic acid, and chlorogenic acid are the common products of phenylpropanoid metabolism and flavonoid metabolism. P-coumaric acid and cinnamic acid are the initial metabolites synthesized via the phenylpropanoid metabolic pathway. Moreover, 4CL converts the two metabolites into p-coumaroyl-CoA and cinnamoyl-CoA then goes into flavonoid metabolism (Vanholme et al., 2019). P-coumaric acid, cinnamic acid, and chlorogenic acid showed a negative correlation with flavonoid metabolites in the high eleutheroside B plants, while chlorogenic acid showed a negative correlation with flavonoid metabolites in the low eleutheroside B plants.

3.4. The regulatory network of genes and metabolites in three secondary metabolic pathways

PCC between DEGs and DAMs participating in phenylpropanoid, flavonoid, and triterpenoid metabolic pathways were calculated to analyze whether the change between gene expression and metabolite accumulation was synergistic (Figure 7; Supplementary Table 10).

Seven DEGs (*PAL3*, *PAL5*, *C4H*, *C3′H1*, *CCoAOMT*, *COMT*, *β-AS*) were identified and were significantly correlated (PCC>0.8, $P < 0.01$) with 53 types of DAMs participating in the above metabolic pathways (Figure 7). A strong correlation (PCC>0.9) was noted between these DEGs and DAMs. Five *PAL* genes were differentially expressed in the high and low eleutheroside B plants. *PAL3* was correlated with only 3-O-ara-oleanolic acid-20(29)-ene-28-O-glc-glc-rha. *PAL5* demonstrated a positive

Figure 7. Correlation network in DEGs and DAMs. Pentagon and circle represent genes and metabolites, respectively. The purple, orange and green circles represent metabolites involved in phenylpropanoid, flavonoid, and triterpenoid metabolism, respectively. The circle with red and black borders indicate significantly higher and lower (VIP>1) metabolite accumulation, respectively, in the high eleutheroside B plants than that in the low eleutheroside B plants. Red and blue lines indicate significantly positive and negative correlations. Corresponding metabolites information is shown in the Supplementary Table 13.

correlation with esculin, prunetin, and two upregulated metabolites. The other three *PAL* genes were not correlated with DAMs involved in phenylpropanoid, flavonoid, and triterpenoid metabolic pathways. *C3′H1* showed a positive correlation with only petasiphenone and a negative correlation with all metabolites (PCC>0.8). Also, *C4H* showed a positive correlation with only petasiphenone, and a negative correlation with hispidulin, jaceosidin, cynarin, and five metabolites. The correlation of DAMs with *CCoAOMT*, *COMT*, and *β-AS* gene accounted for a large proportion of the total correlations between DEGs and DAMs. The above DAMs were involved in 118 metabolites. Eleutheroside B implicated in the phenylpropanoid metabolic pathway showed a positive correlation with *CCoAOMT*, *COMT* gene, while a negative correlation with *β-AS* gene. *PAL3*, *PAL5*, *C3′H1*, and *C4H* genes showed a positive correlation with certain metabolites. Gene expressions and metabolite accumulation were upregulated. Gene expression and content accumulation were downregulated if there was a negative correlation between DEGs and DAMs. *CCoAOMT*, *COMT*, and *β-AS* genes were identified as candidate genes implicated in the eleutheroside B biosynthetic pathway.

3.5. Gene expression in the three developmental stages

Seven types of DEGs (12 genes) were identified in the eleutheroside B biosynthetic pathway (Figure 4). *PAL1*, *C4H* were randomly selected from 12 genes. Meanwhile, *LAR* and *GPS* were selected from flavonoid and triterpenoid metabolic pathways. qRT-PCR was used to establish the gene expression level at the three developmental stages in the high and low eleutheroside B plants.

C4H gene was the highest at the ageing stage and significantly higher than that at the young and mature stages in the high eleutheroside B plants. Moreover, *C4H* expression showed a gradually increasing trend with leaf development (Figure 8E). *GPS* gene expression was highest at the mature stage and significantly higher than that at the young and ageing stages (Figure 8F). *PAL1* gene had the highest expression at the mature stage while its expression at the young stage was significantly lower than that at mature and ageing stages in the high eleutheroside B plants (Figure 8G). Expression of the *LAR* gene was only at the mature stage (Figure 8H).

C4H gene expression was highest at the young stage and lowest at the mature stage in the low eleutheroside B plants. *C4H* expression was upregulated at the mature to ageing stages (Figure 8E). *GPS* gene expression was highest at the young stage and significantly higher than at the mature and ageing stages in the low eleutheroside B plants (Figure 8F). *PAL1* gene had the highest expression at the young stage (Figure 8G). *LAR* gene expression was only at the young stage (Figure 8H). The expression patterns of the *PAL1*, *C4H*, *GPS*, and *LAR* genes were different in the high and low eleutheroside B plants. The above four genes had higher expression levels at the young stage in the low eleutheroside B plants but lower expression levels in the high eleutheroside B plants.

EsABC1, *EsABC4*, *EsABC5* genes were highest at the mature stage in the low eleutheroside B plants (Figure 8). *EsABC2* was lowest at the mature stage in the low eleutheroside B plants. *EsABC3* was highest at the ageing stage and significantly higher than ($P < 0.05$) at the young and mature stages in the low eleutheroside B plants. *EsABC1*, *EsABC2*, *EsABC3*, *EsABC5* genes were the highest at the ageing stage in the high eleutheroside B plants (Figure 8). *EsABC4* gene at the mature stage and significantly higher than ($P < 0.05$) at the young and ageing stages in the high eleutheroside B plants.

3.6. Eleutheroside B content accumulation at three developmental stages

The UPLC system was used to detect eleutheroside B content at the three developmental stages in the high and low eleutheroside B plants (Supplementary Table 1). The eleutheroside B content was highest at the young stage reaching 43.359 μg/g and 18.904 μg/g in high and low eleutheroside B plants, respectively (Figure 8J). The eleutheroside B content demonstrated a gradually decreasing trend with leaf development in the high eleutheroside B plants, which was highest at the young stage > mature stage > senescence stage. Eleutheroside B content was lowest at the mature stage reaching 9.469 μg/g in the low eleutheroside B plants. Eleutheroside B content decreased between the young and mature

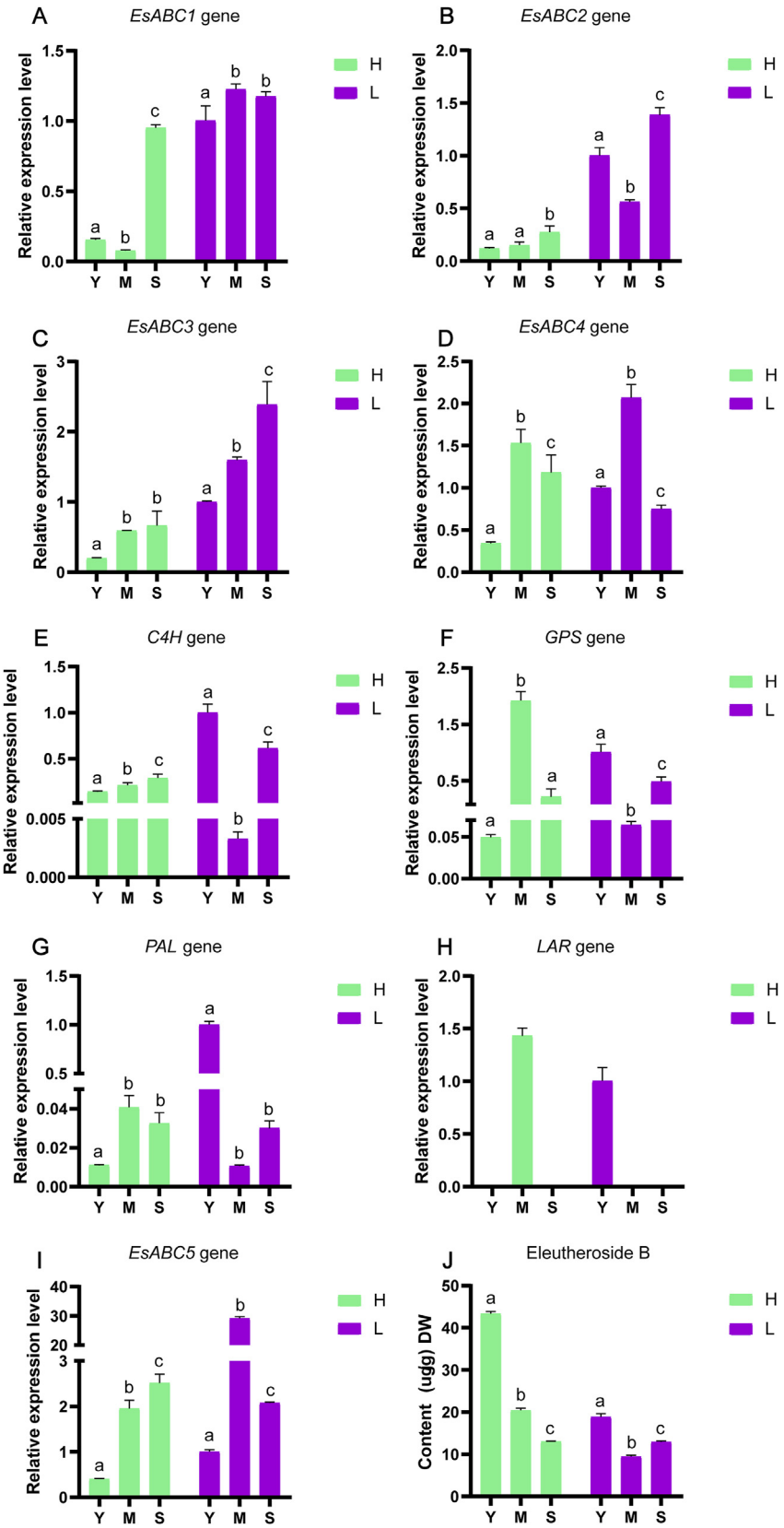

Figure 8. (A)–(I) qRT-PCR analysis of gene expression patterns at three developmental stages in the high and low eleutheroside B plants. (J) Eleutheroside B content at the three developmental stages in the high and low eleutheroside B plants. H and L represent the high and low eleutheroside B plants. Y, M, S represent *E. senticosus* leaf samples at young, mature, and ageing stages, respectively. Different lowercase letters represent significant differences within plants ($P < 0.05$).

stages and increased to 12.931 μg/g between the mature to ageing stages. Eleutheroside B content showed a significant difference at young and mature stages between the high and low eleutheroside B plants. Nevertheless, eleutheroside B content showed no significant difference at the ageing stage.

3.7. Analysis of transcription factors

Transcription factors (TFs) are involved in growth, development, biotic and abiotic stress processes, as well as in the synthesis of secondary metabolites. DEGs encoding transcription factors in the high and low eleutheroside B plants were identified to analyze the TFs potentially involved in the regulation of eleutheroside B synthesis. A total of 43 classes of TFs (140 genes) were identified in the high- and low eleutheroside B plants, including 14 NAC TFs, 9 MYB TFs, 8 MADS TFs and 8 HSF TFs were identified in the high and low eleutheroside B plants (Supplementary Figure 7; Supplementary Table 11). NAC (Li and Cheng et al., 2019), MYB (Geng et al., 2020), homeobox (HB) (Testone et al., 2012), WRKY (Wang et al., 2010); TFs are involved in the lignin synthesis regulation. The lignin and eleutheroside B biosynthetic processes belong to the phenylpropanoid metabolism and overlap between the two processes. The gene expression patterns of the four TFs were analyzed, and consequently, the transcription factors possibly involved in the regulation of the eleutheroside B biosynthetic pathway were identified. A total of 14 genes were identified in the encoding *NAC* TFs of which nine genes were highly expressed in the high eleutheroside B plants (Figure 9), consistent with the accumulation pattern of eleutheroside B content. A total of nine genes encoded the *MYB* TFs. Unlike the accumulation pattern of eleutheroside B content, only *MYB5* and *MYB8* were highly expressed in the low eleutheroside B plants (Figure 9). Consistent with the accumulation pattern of eleutheroside B content, two genes encoding WRKY TFs were highly expressed in the high eleutheroside B plants (Figure 9). Of note, the expression patterns of genes encoding HB TFs were either upregulated or downregulated (Figure 9).

NAC, MYB, HB, WRKY TFs participated in the eleutheroside B biosynthetic pathway and other secondary metabolic pathways. We analyzed the correlation between the four DEGs encoding TFs and DAMs involved in phenylpropanoid, flavonoids, and triterpenoid metabolic pathways (Supplementary Table 12). Two genes encoding WRKY TFs showed no correlation with DAMs involved in phenylpropanoid, flavonoids, and triterpenoid metabolic pathways. *NAC5* and *NAC7* genes encoding TFs showed a significant correlation (PCC>0.9, $P < 0.01$) with metabolites implicated in triterpenoid metabolic pathways including ciwujianoside C3 and ciwujianoside D1 (Figure 10). *NAC5* and *NAC7* genes showed a significant correlation with seven and two metabolites involved in the flavonoid metabolic pathway, respectively. *NAC5* gene showed a positive correlation with eleutheroside B with consistent gene expression and content accumulation patterns. However, *NAC7* was not

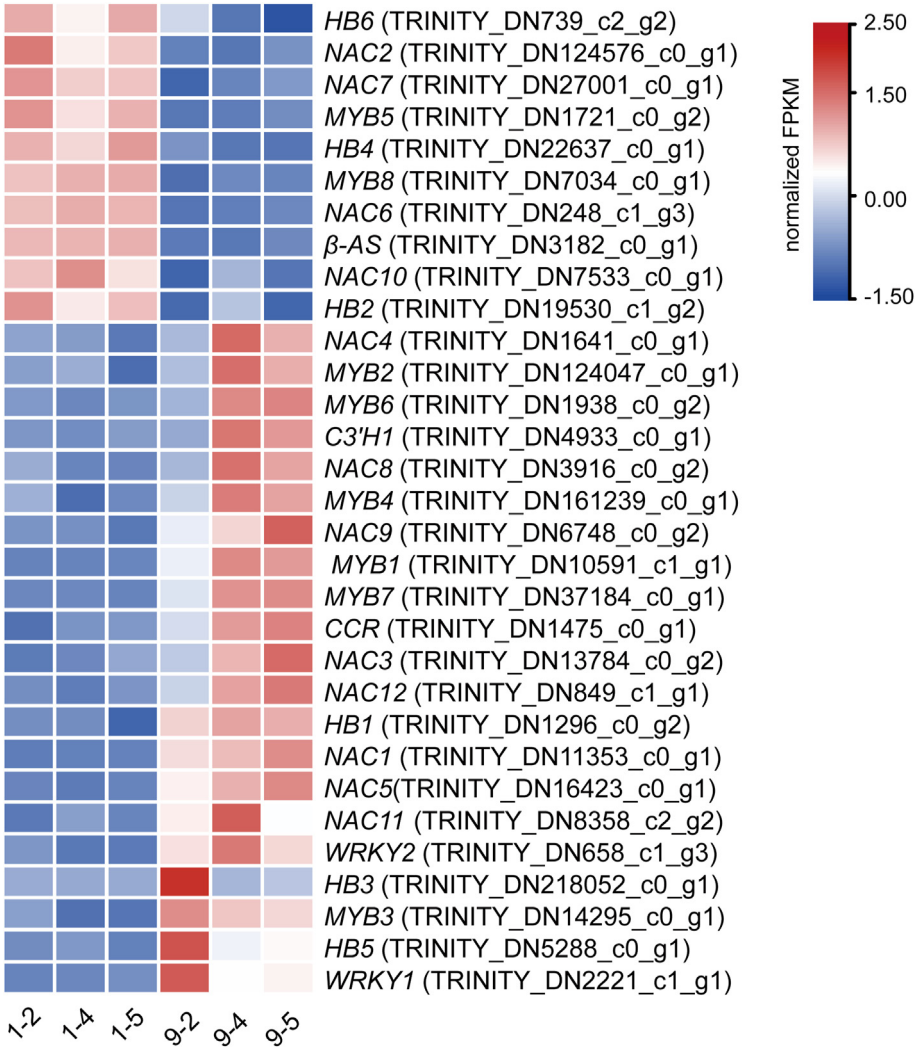

Figure 9. Heat map expression patterns of DEGs encoding *NAC*, *MYB*, *HB*, and *WRKY* TFs. Each colored cell represents a normalized FPKM value (three biological replicates). The color scale from blue (low) to red (high) represents gene expression levels.

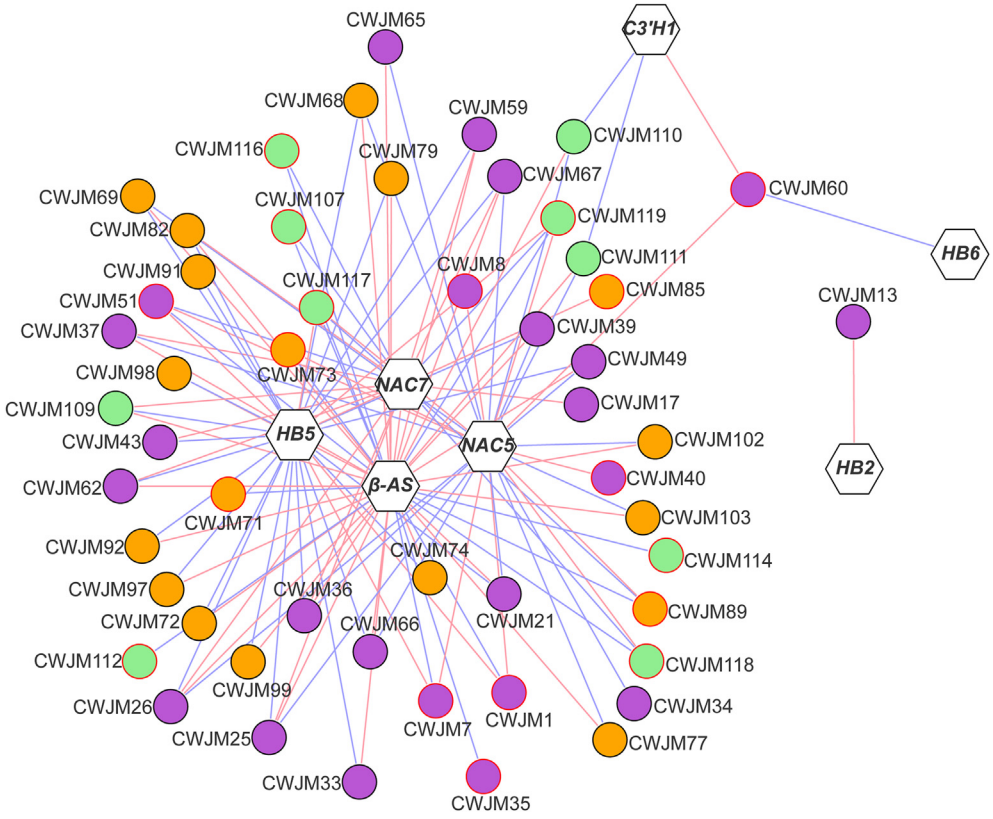

Figure 10. Correlation network in DEGs encoding TFs and DAMs. Pentagon and circle represent genes and metabolites, respectively. Purple, orange, and green circles represent the metabolites involved in phenylpropanoid, flavonoid, and triterpenoid metabolism, respectively. Circle with red and black borders indicate significantly higher and lower (VIP>1) metabolite accumulation, respectively, in the high eleutheroside B plants than that in the low eleutheroside B plants. Red and blue lines indicate significantly positive and negative correlations. Corresponding metabolite information is shown in the Supplementary Table 13.

correlated with eleutheroside B. *HB5* gene encoding TFs showed a significant correlation with metabolites involved in flavonoid and triterpenoid metabolism pathways. *HB5* gene showed a positive correlation with eleutheroside B with consistent gene expression and content accumulation patterns. NAC5 and HB5 TFs may positively regulate the synthesis of eleutheroside B.

4. Discussion

4.1. Relationship between DEGs and DAMs in the eleutheroside B biosynthetic pathway

The synthesis of eleutheroside B had been predicted. Aaromatic amino acids L-phenylalanine and L-tyrosine, produced via the shikimic acid pathway, are further converted into a series of cinnamic acid derivatives. Lignin and lignans are formed by phenolic oxidative coupling of 4-hydroxycinnamyl alcohol monomers, as p-coumaryl alcohol, coniferyl alcohol, and sinapyl alcohol. During the synthesis of syringin, ferulic acid is converted into 5-hydroxyferulic acid, then into sinapic acid, sinapoyl Co-A, and sinapaldehyde via series of reduction reactions. Cinnamyl alcohol dehydrogenase further converts sinapaldehyde into sinapyl alcohol, finally eleutheroside B by coupling sinapyl alcohol and glucose, and catalyzed by glucosyltranferase (Murthy et al., 2014).

Widely targeted metabolome analysis revealed the presence of DAMs in other secondary metabolic pathways, except phenylpropanoid metabolism. PCA and OPLS-DA results identified that samples could be divided into two plants and that metabolites in these plants are different. Thus, the accumulation of metabolites implicated in phenylpropanoid, triterpenoid, and flavonoid metabolisms are different. Comparisons of metabolites in the high and low eleutheroside B plants revealed 161 metabolites with a significant difference. Moreover, gene expression levels showed significant differences between the two plants. *PAL*, *C4H*, *C3′H*, *CSE*, *COMT*, *CCoAOMT*, and *CCR* gene expressions were higher in the high eleutheroside B plants (Figure 4) and the correlation analysis of DEGs and DAMs revealed a positive correlation between eleutheroside B accumulation levels and *CCoAOMT, COMT* gene expression levels (Figure 7). Nonetheless, corresponding levels of enzymes involved in the synthesis of various metabolites synthesis of metabolites, including chlorogenic acid, sinapyl alcohol, caffeic acid, cinnamic acid, and p-coumaric acid did not show a significant difference when gene expression levels were up regulated (Figure 4). Consistent with accumulation patterns of cinnamic acid, p-coumaric acid, and ferulic acid (Cuong et al., 2018), *McPAL*, *Mc4H*, and *McCOMT* genes in bitter melon are highly expressed in leaves. This indicates that the precursors for the synthesis of eleutheroside B are competed by other pathways, but in the late stages of eleutheroside B synthesis, the intermediate metabolites are used exclusively for the production of eleutheroside B, thus exhibiting a strong correlation between genes and metabolites.

Eleutheroside B is a monolignol glycoside synthesized via the phenylpropanoid metabolic pathway. Nevertheless, the biosynthetic process of eleutheroside B has not been established (Murthy et al., 2014). The eleutheroside B biosynthetic pathway was predicted using the identified combined lignin biosynthetic pathways, genes, and metabolites (Figure 4) (Dixon and Barros, 2019; Vanholme et al., 2019). Also, we investigated the process of eleutheroside B synthesis proposed by Murthy. Subsequently, another eleutheroside B biosynthetic pathway in *E. senticosus* was proposed. Two branched pathways exist, including 4CL mediated synthesis of p-coumaroyl-CoA from p-coumaric acid and synthesis of caffeic acid from p-coumaric acid; HCT mediated synthesis of p-coumaroyl quinic acid and p-coumaroyl shikimate from p-coumaroyl-CoA; C3′H mediated synthesis of chlorogenic acid and 5-O-caffeoyl shikimic acid from p-coumaroyl quinic acid and p-coumaroyl shikimate. Moreover, HCT and CSE convert 5-O-caffeoyl shikimic acid into caffeoyl-CoA and caffeic acid, respectively. The above process contains multiple branching steps. *CCoAOMT*, *COMT*, *F5H*, *CCR*, and *CAD* convert caffeic acid into caffeyl alcohol, coniferyl alcohol, 5-hydroxyconiferyl alcohol, and sinapyl alcohol, respectively. Then, the coniferyl alcohol, 5-hydroxyconiferyl alcohol, and sinapyl alcohol are converted into guaiacyl (G)-unit-enriched lignin polymer, 5-hydroxyguaiacyl (5HG) -unit-enriched lignin polymer, and syringyl (S)-unit-enriched lignin

polymer, respectively. Ultimately, GT mediates the synthesis of eleutheroside B from sinapyl alcohol. *E. senticosus* contains abundant secondary metabolites, and the synthesis of these secondary metabolites affects each other. Which resulted in a poor correlation between genes and corresponding metabolites in the early stages of eleutheroside B synthesis, but a strong correlation between genes (*COMT* and *CCOMT*) and eleutheroside B existed in the late stages of eleutheroside B synthesis. In this study, we integrated lignin biosynthesis and all possible branch pathways for eleutheroside B biosynthesis based on the prediction process of eleutheroside B synthesis (Murthy et al., 2014; Dixon and Barros, 2019; Vanholme et al., 2019). This was to establish a relatively complete biosynthetic pathway. DEGs were identified in the two-branched pathways of eleutheroside B biosynthesis and both could be the eleutheroside B biosynthetic pathway (Figure 4).

4.2. Gene expression patterns in the eleutheroside B biosynthetic process

Two *C3′H* genes (*C3′H1*, *C3′H2*) were selected from the high and low eleutheroside B plants. Their expressions were upregulated in the high eleutheroside B plants. C3′H mediates the synthesis of chlorogenic acid and 5-O-caffeoyl shikimic acid from p-coumaroyl quinic acid and p-coumaroyl shikimate, respectively. *C3′H*, in *Morus alba* L., was differentially expressed before and after frost. Expression levels of *C3′H* were positively correlated with accumulation levels of chlorogenic acid (Zhao et al., 2019). *C3′H1* was positively correlated with petasiphenone only. Gene expression levels were consistent with accumulation patterns of this metabolite in *E. senticosus*. However, no correlation was noted between *C3′H1* and chlorogenic acid. In the eleutheroside B biosynthetic pathway, HCT mediates the synthesis of p-coumaroyl quinic acid and p-coumaroyl shikimate from p-coumaroyl-CoA. Enzymatic assays have shown that *MaHCT4* uses quinic acid as an acyl acceptor (Zhao et al., 2019). Nevertheless, the pathway of the two branching processes catalyzed by HCT in *E. senticosus* has not been established.

Of note, the eleutheroside B biosynthetic pathway and lignin synthesis processes mostly overlap. Although genome sequencing of *Panax ginseng* C. A. Mey (Xu et al., 2017) and *Panax notoginseng* (Burk.) F. H. Chen (Jiang et al., 2021) have been performed, genes implicated in lignin synthesis remain unreported. As such, the process of lignin synthesis in *Araliaceae* is unknown. Furthermore, no reference on the genes involved in the lignin biosynthesis process in *E. senticosus* has been reported. Herein, DEGs and DAMs of the eleutheroside B biosynthetic pathway were identified using metabolomic approaches in the high and low eleutheroside B plants. This study illuminates gene sequences, metabolite accumulation, levels, and the relationship between gene expression and metabolite accumulation, thus laying a basis for exploring the molecular mechanisms affecting eleutheroside B synthesis.

4.3. TFs analysis in the eleutheroside B high content and low eleutheroside B plants

A total of 43 types of TFs were identified in the high and low eleutheroside B plants. NAC TFs regulate gene expressions related to lignin monomer synthesis via the downstream cascade reaction of TFs (Liu et al., 2015; Ohtani and Demura, 2019). *OsSWN* and *ZmSWN* genes, which encode NAC TFs in rice and maize activate secondary wall-related TFs and gene expression of secondary wall synthesis (Zhong et al., 2011). *OsSWN* and *ZmSWN* TFs combine with the NAC binding element (SNBE) of *OsMYB46* and *ZmMYB46* promoters to directly activate their expression. Lignin synthesis-associated *NAC*, *HB*, *MYB*, and *WRKY* genes, which encode TFs were identified. NAC TFs possibly combine with *C3′H2*, *CCoAOMT*, *COMT,* and other gene promoters involved in eleutheroside B and lignin biosynthetic processes to activate gene expression. In *A. thaliana*, *MYB63* and *MYB85* act as specific lignin activators to induce *CSE* expression (Vargas et al., 2016). The seven MYB TFs identified in this study may be implicated in *CSE* positive transcription regulation.

4.4. Gene expression levels and eleutheroside B accumulation at the three developmental stages

PAL and *C4H* gene expression levels at the young, mature, and ageing stages were inconsistent with accumulation patterns of eleutheroside B, indicating a complex relationship between genes and metabolites. Eleutheroside B content was highest at the young stage both in the high and low eleutheroside B plants. We compared eleutheroside B concentrations during the five harvesting periods between June to October (Li and Fu et al., 2019). As a result, eleutheroside B content was highest in early July. Eleutheroside B concentrations were the highest between the young to mature stages (Figure 8J).

In the high eleutheroside B plants, eleutheroside B concentrations gradually decreased as the leaves age. Nevertheless, the cause of this phenomenon is unknown. Previous studies indicate that triterpene saponin concentrations in the roots, stems, leaves, and petioles of *E. senticosus* correlate with the pleiotropic drug resistance (PDR) transporter (Xing et al., 2014). ATP-binding cassette (ABC) and multidrug and toxin extrusion (MATE) transporters can complete membrane transport of secondary metabolites in plants (Gani et al., 2021). In the high eleutheroside B plants, *EsABC2, EsABC3*, and *EsABC5* gene expression were gradually upregulated as leaves aged, whereas eleutheroside B concentrations gradually decreased. These 3 transporters may be responsible for the membrane transport of eleutheroside B. Eleutheroside B accumulation in the leaves could be attributed to membrane transport as the leaves age. Thus, the difference of eleutheroside B concentrations in various plant tissues potentially correlates with the membrane transport of secondary metabolites. However, eleutheroside B concentrations and transport in different tissues of *E. senticosus* should be further investigated to exhaustively explore eleutheroside B accumulation.

Declarations

Author contribution statement

Hong-Yu Guo: Conceived and designed the experiments; Analyzed and interpreted the data; Wrote the paper.

Jie Zhang, Li-Mei Lin, Xin Song: Performed the experiments.

Duo-Duo Zhang, Ming-Hui Cui, Chang-Wen Long: Analyzed and interpreted the data.

YueHong Long, Zhao-Bin Xing: Conceived and designed the experiments.

Funding statement

This work was supported by Natural Science Foundation of Hebei Province (H2020209302), Science and Technology Project of Hebei Education Department (ZD2019075), The National Natural Science Foundation of China (Grant No. 31570683), and Research Project of Fundamental Scientific Research Business Expenses of Provincial Colleges and Universities in Hebei Province (JXC2019002).

Data availability statement

Data associated with this study has been deposited at GenBank under the accession number [GenBank MZ054641, GenBank MZ054642, GenBank MZ054643, GenBank MZ054644].

Data associated with this study has been deposited at NCBI SRA Datasets under the accession number PRJNA728574.

Declaration of interests statement

The authors declare no conflict of interest.

Additional information

Supplementary content related to this article has been published online at doi:.10.1016/j.heliyon.2022.e09665

References

Chen, W., Gong, L., Guo, Z., Wang, W., Zhang, H., Liu, X., et al., 2013. A novel integrated method for large-scale detection, identification, and quantification of widely targeted metabolites: application in the study of rice metabolomics. Mol. Plant 6, 1769–1780.

Cui, Y., Zhang, Y., Liu, G., 2015. Syringin may exert sleep-potentiating effects through the NOS/NO pathway. Fundam. Clin. Pharmacol. 29, 178–184.

Cuong, D.M., Kwon, S.-J., Jeon, J., Park, Y.J., Park, J.S., Park, S.U., 2018. Identification and characterization of phenylpropanoid biosynthetic genes and their accumulation in bitter melon (*Momordica charantia*). Molecules 23, 469.

Dai, R., Niu, M., Wang, N., Wang, Y., 2021. Syringin alleviates ovalbumin-induced lung inflammation in BALB/c mice asthma model via NF-κB signaling pathway. Environ. Toxicol. 36, 433–444.

Dixon, R.A., Barros, J., 2019. Lignin biosynthesis: old roads revisited and new roads explored. Open Biol. 9, 190215.

Gani, U., Vishwakarma, R.A., Misra, P., 2021. Membrane transporters: the key drivers of transport of secondary metabolites in plants. Plant Cell Rep. 40, 1–18.

Geng, D., Shen, X., Xie, Y., Yang, Y., Bian, R., Gao, Y., et al., 2020. Regulation of phenylpropanoid biosynthesis by MdMYB88 and MdMYB124 contributes to pathogen and drought resistance in apple. Hortic. Res. 7, 102.

Guo, H., Lao, F., Li, Z., You, P., Xing, Z., Long, Y., 2017. Cloning and analysis of squalene synthase gene DNA and promoter in *Eleutherococcus senticosus*. Mol. Plant Breed. 15, 1289–1294.

Huang, L., Zhao, H., Huang, B., Zheng, C., Peng, W., Qin, L., 2011. *Acanthopanax senticosus*: review of botany, chemistry and pharmacology. Pharmazie 66, 83–97.

Huang, X., Liu, Y., Zhang, X., 2017. Advances in chemical constituents, pharmacological effects and modern clinical application of acanthopanax senticosus leaves. J. Clin. Med. 37, 611–613.

Hwang, H.-S., Lee, H., Choi, Y.E., 2015. Transcriptomic analysis of Siberian ginseng (*Eleutherococcus senticosus*) to discover genes involved in saponin biosynthesis. BMC Genom. 16, 180.

Jiang, Z., Tu, L., Yang, W., Zhang, Y., Hu, T., Ma, B., et al., 2021. The chromosome-level reference genome assembly for *Panax notoginseng* and insights into ginsenoside biosynthesis. Plant Commun. 2, 100113.

Kim, B., Kim, M.-S., Hyun, C.-K., 2017. Syringin attenuates insulin resistance via adiponectin-mediated suppression of low-grade chronic inflammation and ER stress in high-fat diet-fed mice. Biochem. Biophys. Res. Commun. 488, 40–45.

Lee, C.-H., Huang, C.-W., Chang, P.-C., Shiau, J.-P., Lin, I.-P., Lin, M.-Y., et al., 2019. Reactive oxygen species mediate the chemopreventive effects of syringin in breast cancer cells. Phytomedicine 61, 152844.

Li, J.-P., Fu, S.-P., Wang, Q.-B., Wang, C., Zhao, T.-Q., Wang, Z.-Y., 2019a. Comprehensive evaluation of suitable harvesting period of *Acanthopanax Senticosus* leaves by multiple indicators. Chin. Tradit. Herb. Drugs 50, 3187–3192.

Li, M., Cheng, C., Zhang, X., Zhou, S., Wang, C., Ma, C., et al., 2019b. *PpNAC187* enhances lignin synthesis in 'Whangkeumbae' pear (*Pyrus pyrifolia*) 'Hard-End' fruit. Molecules 24, 4338.

Liu, J., Osbourn, A., Ma, P., 2015. MYB transcription factors as regulators of phenylpropanoid metabolism in plants. Mol. Plant 8, 689–708.

Livak, K.J., Schmittgen, T.D., 2001. Analysis of relative gene expression data using real-time quantitative PCR and the 2(-Delta Delta C(T)) Method. Methods 25, 402–408.

Long, Y.-H., Li, F.-F., Yang, G., Xing, Z.-B., 2015. Gene cloning and expression level of bAS and their correlation with content of saponins in *Eleutherococcus senticosus*. Chin. Tradit. Herb. Drugs 46, 1354–1359.

Meng, X.-C., Yan, B.-P., Sun, H., Wang, X.-J., 2009. Study on effective constituent contentsin different positions and tissues of *Acanthopanax senticosus*. Lishizhen Med. Mater. Med. Res. 20, 1899–1900.

Murthy, H.N., Kim, Y.-S., Georgiev, M.I., Paek, K.-Y., 2014. Biotechnological production of eleutherosides: current state and perspectives. Appl. Microbiol. Biotechnol. 98, 7319–7329.

Ohtani, M., Demura, T., 2019. The quest for transcriptional hubs of lignin biosynthesis: beyond the NAC-MYB-gene regulatory network model. Curr. Opin. Biotechnol. 56, 82–87.

Shen, Z., Yang, C., Zhu, P., Tian, C., Liang, A.F., 2020. Protective effects of syringin against oxidative stress and inflammation in diabetic pregnant rats via TLR4/MyD88/NF-κB signaling pathway. Biomed. Pharmacother. 131, 110681.

Song, J., Guo, H.-Y., Li, Z.-D., You, P.-S., Long, Y.-H., Xing, Z.-B., 2016. Analysis of transicriptomes and differentially expressed genes in *Eleutherococcus senticosus*. Chin. Tradit. Herb. Drugs 47, 4049–4053.

Testone, G., Condello, E., Verde, I., Nicolodi, C., Caboni, E., Dettori, M.T., et al., 2012. The peach (*Prunus persica* L. Batsch) genome harbours 10 *KNOX* genes, which are differentially expressed in stem development, and the class 1 *KNOPE1* regulates elongation and lignification during primary growth. J. Exp. Bot. 63, 5417–5435.

The State Pharmacopoeia Commission of P.R. China, 2015. Pharmacopoeia of the People's Republic of China. China Medical Science Press, Beijing.

Vanholme, R., De, M.B., Ralph, J., Boerjan, W., 2019. Lignin biosynthesis and its integration into metabolism. Curr. Opin. Biotechnol. 56, 230–239.

Vargas, L., Cesarino, I., Vanholme, R., Voorend, W., De Lyra Soriano Saleme, M., Morreel, K., et al., 2016. Improving total saccharification yield of Arabidopsis plants by vessel-specific complementation of *caffeoyl shikimate esterase* (*cse*) mutants. Biotechnol. Biofuels 9, 139.

Wang, C.Y., Zhang, Q., Xun, Z., Yuan, L., Li, R., Li, X., et al., 2020. Increases of iASPP-Keap1 interaction mediated by syringin enhance synaptic plasticity and rescue cognitive impairments *via* stabilizing Nrf2 in Alzheimer's models. Redox Biol. 36, 101672.

Wang, H., Avci, U., Nakashima, J., Hahn, M.G., Chen, F., Dixon, R.A., 2010. Mutation of WRKY transcription factors initiates pith secondary wall formation and increases stem biomass in dicotyledonous plants. Proc. Natl. Acad. Sci. U. S. A 107, 22338–22343.

Wang, Z., Guo, H., Zhang, Y., Lin, L., Cui, M., Long, Y., et al., 2019. DNA methylation of farnesyl pyrophosphate synthase, squalene synthase, and squalene epoxidase gene promoters and effect on the saponin content of *Eleutherococcus Senticosus*. Forests 10, 1053.

Wang, Z.-B., Guo, J.-T., Jiang, H., Yang, B.-Y., Kuang, H.-X., 2013. Study on the chemical constituents and pharmacological effects of *Acanthopanax senticosus* leaves. Infor. Trad. Chin. Med. 30, 29–32.

Wu, K.-X., Liu, J., Liu, Y., Guo, X.-R., Mu, L.-Q., Hu, X.-H., et al., 2018. A comparative metabolomics analysis reveals the tissue-specific phenolic profiling in two *Acanthopanax* species. Molecules 23, 2078.

Xing, Z.-B., Lao, F.-Y., Long, Y.-H., Liang, N.-S., Chen, L., He, S., 2012. Single nucleotide polymorphism of squalene synthase and squalene epoxidase genes and their correlation with content of saponins in *Eleutherococcus senticosus*. Chin. Tradit. Herb. Drugs 43, 2020–2024.

Xing, Z.-B., Meng, C.-Y., Xiu, L.-S., Lao, F.-Y., Zhuang, P.-Y., Chai, L.-H., 2014. Cloning of pleiotropic drug resistance transporter gene from *Eleutherococcus senticosus* and effect of its expression on saponins content. J. Zhejiang Agric. Univ. 26, 351–355.

Xu, J., Chu, Y., Liao, B., Xiao, S., Yin, Q., Bai, R., et al., 2017. *Panax ginseng* genome examination for ginsenoside biosynthesis. GigaScience 6, 1–15.

Zhang, H., Gu, H., Jia, Q., Zhao, Y., Li, H., Shen, S., et al., 2020. Syringin protects against colitis by ameliorating inflammation. Arch. Biochem. Biophys. 680, 108242.

Zhang, Y.-S., 2009. *Acanthopanax senticosus* and hygienical efficacy, processing techniques of *A. senticosus* tea. Sub. Agric. R. 5, 56–59.

Zhao, L., Wang, D., Liu, J., Yu, X., Wang, R., Wei, Y., et al., 2019. Transcriptomic analysis of key genes involved in chlorogenic acid biosynthetic pathway and characterization of *MaHCT* from *Morus alba* L. Prot. Exp. Purif. 156, 25–35.

Zhong, R., Lee, C., McCarthy, R.L., Reeves, C.K., Jones, E.G., Ye, Z.-H., 2011. Transcriptional activation of secondary wall biosynthesis by rice and maize NAC and MYB transcription factors. Plant Cell Physiol. 52, 1856–1871.